Applied Ecology and Environmental Sciences, 2021, Vol. 9, No. 3, 356-367
Available online at http://pubs.sciepub.com/aees/9/3/6
Published by Science and Education Publishing
DOI:10.12691/aees-9-3-6

Preparation and Characterization of Clay/Urea Formaldehyde Resin Composites

Swati Kalra*, G.P. Singh

Department of Physics, Govt. Dungar College, Bikaner 334001 Rajasthan, India
*Corresponding author: swati.kalra1986@gmail.com

Received February 14, 2021; Revised March 17, 2021; Accepted March 22, 2021

Abstract Composites of urea-formaldehyde/clay were synthesized and analyzed in the present study. The analyses of XRD, FTIR, DSC, and TGA were performed to investigate the variation of urea-formaldehyde (UF)/clay composites' structural and thermal properties with different clay loading levels. It was discovered that the clay loading level influences the glass transition temperature of UF resin. Thermo Gravimetric Analysis (TGA) has shown that the degree of clay loading and heating rate affects the composites' thermal stability. Furthermore, the curing reactions' activation energy was investigated using Kissinger's and Ozawa's methods, confirming the presence of interactions between the polymer chain and clay particles.

Keywords: *clay, urea-formaldehyde, composites, FTIR, XRD, TGA, DSC*

Cite This Article: Swati Kalra, and G.P. Singh, "Preparation and Characterization of Clay/Urea Formaldehyde Resin Composites." *Applied Ecology and Environmental Sciences*, vol. 9, no. 3 (2021): 356-367. doi: 10.12691/aees-9-3-6.

1. Introduction

Clay is defined as a small crystal of alumino silicates of different ratios, having a substitution of iron and magnesium by alkali and alkaline earthy elements [1]. Most of the clay is found as a natural rocks or soils that include many minerals. Generally, clay is a fine material separated from other materials by composition structure and size. The dispersion amount of clay in clay/polymer composites is developed along with many better properties. These composites have improved properties compared to the plane polymer matrix. PCN (polymer clay composites) is generally prepared by using clay of nano or micro range. Only a small quantity of clay dispersed into the matrix can make an excellent increment in conventional polymers' properties. High clay loading level reduced the polymer's strength and toughness [2,3,4,5,6]. In this way, the addition of clay into the polymers comes with a value-added material. In the coating materials, the presence of organoclay alleviate the rheological properties of the coating material. This formatted coating material would control the pigment settling and sink on surfaces [7]. Many studies have been done on clay's ability to boost the properties of the material [8,9,10]. Thermal properties of grease with clay are also studied. It is concluded that the addition of organoclay improved the thermal properties [11,12]. Moreover, nano clay also has an application in cosmetics and ink due to its color retention [7,13]. Petroleum industries also use organoclay to remove the hydrocarbon from refineries [13]. Again for pharmaceuticals and pesticide industries, clay is used to remove toxic chemicals. Due to clay's absorption properties, it is also used to remove heavy metals, polychlorinated biphenyl, and organic materials [14], for removal of radionuclide's from water [15,16] and application as a therapeutic agent drug vehicle [17]. The innovator of nanocomposite science is the Toyota company research group. This company's research group successfully prepared Nylon6 nanocomposites with excellent properties [18]. For the enhancement of these properties, clay is proposed as a filler. Under heat operations, the order of thermal expansion is as follows:

Polymer > metal > ceramic

Therefore to decrease the thermal expansion and increase the thermal stability clay (ceramics) is used as filler in the polymer matrix. This study includes the preparation of urea-formaldehyde/ball clay composites. The objective of this study is the formation and characterization of urea-formaldehyde/clay composites by using clay with different loading levels. The clay used in this study is locally available ball clay in Bikaner, district of Rajasthan.

2. Experiment Procedure

2.1. Materials

Ball clay sample was collected from industry located in the Bikaner district's kolayat region (western part of Rajasthan). Urea is taken in the form of balls and liquid formaldehyde from Green chemistry laboratory, Dungar College, Bikaner.

2.2. Sample Preparation

Urea was dissolved in formaldehyde (HCHO) and heated at 60^0C for about 2-3 hours with continuous stirring. The mixture was then cast on a flat rectangular Petri dish and left to dry at room temperature to prepare standard urea-formaldehyde to achieve constant weight. For the formation of clay/UF composite (CUF), the same methodology has been followed by mixing ball clay in the mixture. After drying, composites were cut into appropriate dimensions for different tests. For this study, the particle size of used clay is 2 µm. Different clay contents (5 wt%, 10 wt%, 15 wt%, 20 wt%, 25 wt%, 30wt%) of ball clay were used to produce clay-modified composites. The labeling of composites is shown in Table 1.

Table 1. Composition and Labeling of Studied Composites

Clay loading (wt%)	Label of composite
5	CUF 5 B
10	CUF 10 B
15	CUF 15 B
20	CUF 20 B
25	CUF 25 B
30	CUF 30 B

3. Result and Discussion

3.1. FTIR

UF resin is formed when a condensation reaction of urea and formaldehyde takes place. This resin is chemically identified as poly (methylene ether hydroxymethyl ureas). Clay which contains SiO_2 particles has a SiOH group known as silanol group, which may react with macromolecular end groups and mainly with hydroxyl group [19]. During urea and formaldehyde reaction, Dimethylol Urea is produced in which two hydroxyl groups are readily available to interact with silanol groups of SiO_2 [20]. The FTIR spectra of the UF resin is shown in Figure1. The complexity of the polymer structure results in multiple and broad peaks, as shown in this spectra. The broad peak related to the hydrogen-bonded OH and NH group is present around 3300–3350 cm^{-1}. The hydrogen bond is formed between the OH group of monomers (water and formaldehyde) and reactive functional groups CH_2OH, NH_2, and NH [21]. It is mentioned that the peak at 3440 cm^{-1} is the characteristic peak of the free NH_2 group, while the peak at 3340 cm^{-1} is the characteristic peak of bonded NH group [20]. In the pure UF resin spectrum, the peak is found at 3341 cm^{-1} which suggests that the bonded NH group is present in the resin. A weak absorption band appears in the pure UF resin spectrum of 3040-2900 cm^{-1}, attributed to the symmetric CH stretching mode of CH_2, CH_2OH, and NCH_2 [22]. The peak at 1699 cm^{-1} is attributed to the stretching of carbonyl (C=O) (amide I) in the $CONH_2$ group [23]. A weak band at 1471 cm^{-1} and 1346 cm^{-1} may be ascribed to CH bending mode (CH_2 methylene bridges) in $CH_2/CH_2OH/NCH_2N$ [22,23]. A peak at 1245 cm^{-1} is due to CN stretching [24]. The other observed peak at 1138 cm^{-1} and 1035 cm^{-1} are assigned to CO aliphatic ether and methylene bridge (NCH_2N), respectively [25]. The weak and small peak at 770 cm^{-1} is for NH bending and wagging vibration of amide I and amide II, respectively [26].

The FTIR spectra of clay is shown in Figure 2. The band observed at the 3690 cm^{-1} can be attributed to the stretching vibration of AlOH, and the weak band at 3426 cm^{-1} may be assigned to hydroxyl stretching vibrations [27]. The small peak at 2990-2900 cm^{-1} is attributed to CH_2 asymmetric stretching vibration [24]. The peak at 1626 cm^{-1} is related to H-OH bending vibrations of water molecules absorbed on clay [27]. A peak at 1041 cm^{-1} is attributed to the stretching of Si-O-Si bonds [28].

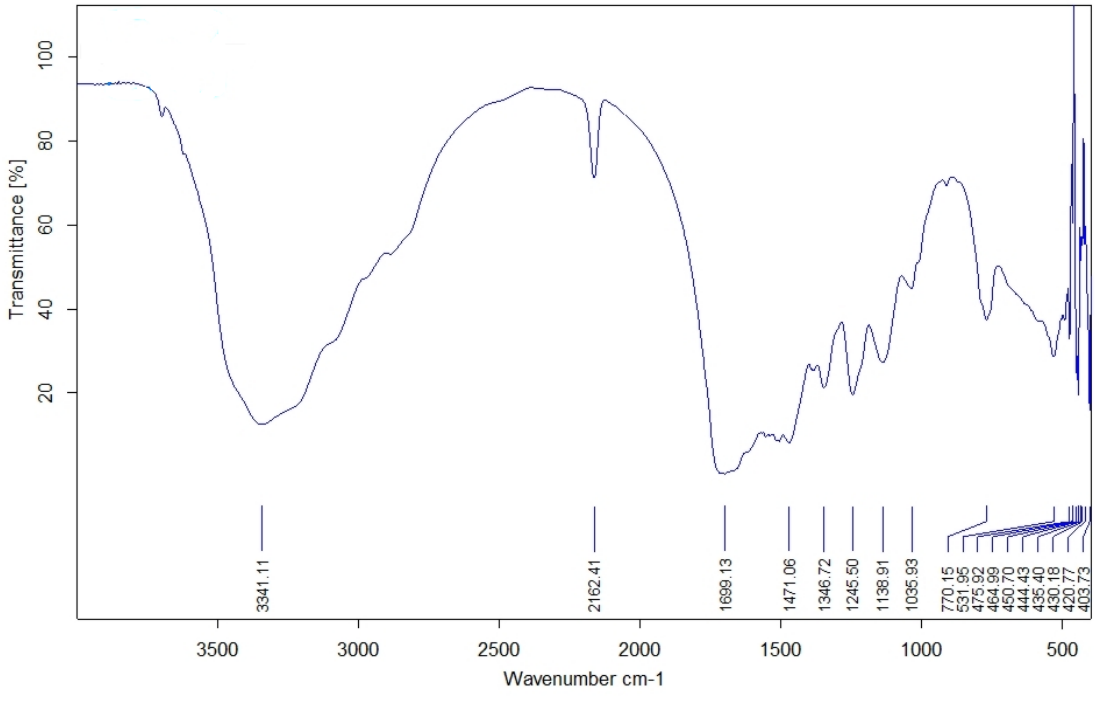

Figure 1. FTIR of UF resin

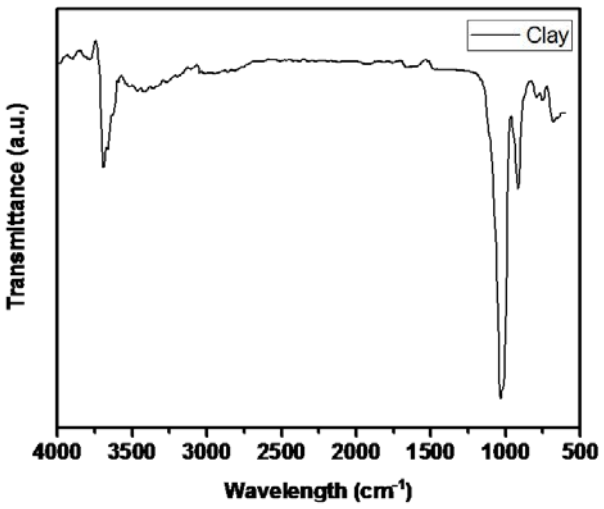

Figure 2. FTIR of clay

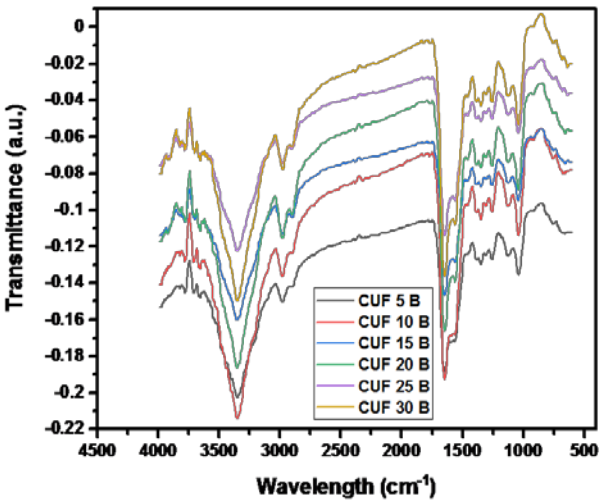

Figure 3. FTIR of CUF composites

Table 2. Assignment of IR absorption peaks for UF and CUF composites

Functional Group	UF	CUF B
hydrogen bonded O-H and N-H band	3341	3348
within phase stretching of -CH_2 hydrocarbon	3040-2900	2984,2893
stretching of carbonyl (-C=O) (amide-I) in $CONH_2$ group	1699	1645
N-H stretching	-	1556
Deformation vibration peak of methylene, C-H bending mode	1471,1346	1348
C-N stretching	1245	1253
asymmetric stretching vibration of -N-CH_2-N group, vibration of (C-O-C), vibration of (Si-O-C) and vibration of asymmetric Si-O-Si of silicone	1138,1035	1150-1130,1039
Si-O-Si deformation	-	758

The FTIR spectra of the CUF composites is shown in Figure 3. All the peaks are shown in the Table 2 for UF resin and CUF composite. The peaks around 3690 cm^{-1} of clay, related to OH stretching vibrations caused by layered silicates, disappeared, which can be due to resin existence inside the layer [24]. The peaks in the range of 3343-3358 cm^{-1} are assigned to stretching of NH bonds formation. The peaks for all the composites in the range of 2963-2874 cm^{-1} are attributed to within phase stretching of CH_2 hydrocarbon, which shows the dispersion of clay platelets that have intercalated the polymer chains [29]. Peaks in the range of 1640-1675 cm^{-1} belong to the NH-C=O group. Peaks in the range of 1537-1593 cm^{-1} are assigned to NH stretching [24]. Peaks observed at 1340-1350 cm^{-1} are the deformation vibration peaks of methylene indicates a further polycondensation reaction in UF resin [28]. Peaks observed in the range of 1236-1253 cm^{-1} for CUF composites are due to CN stretching. In the range of 790-742 cm^{-1}, obtained peaks are due to Si-O-Si deformation [24]. In the range of 1150-1130 cm^{-1} a medium absorption band is obtained which is due to the asymmetric stretching vibration of NCH_2N group, the vibration of (C-O-C), vibration of (Si-O-C) and vibration of asymmetric Si-O-Si of silicone [22].

3.2. XRD

X Ray Diffraction technique is useful for confirming the degree of dispersion of clay in polymer matrices [10]. By using the Bragg equation and XRD test results, the distance between the layers of clay can be calculated. The wavelength of radiation (λ) used was 1.541874 A^0. The interlayer space can be calculated using Bragg's equation which is

$$2dsin\theta = n\lambda$$

where n is the integer number for wavelength (in this case n=1), λ is the wavelength of the X ray, d is the platelet interlayer spacing in A^0, θ is the X ray maximum diffraction angle.

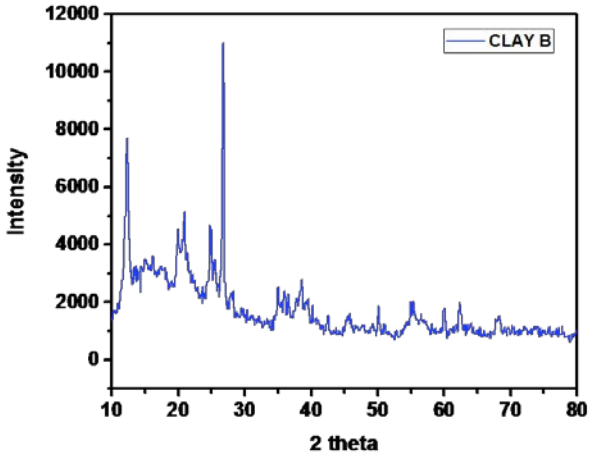

Figure 4. XRD of clay

The XRD spectrum patterns of the ball clay is shown in Figure 4. XRD spectrum of ball clay revealed broad elevated background showing the significant proportion of crystalline constituents, with major mineral phases

identified as SiO_2 with prominent peaks, is about 64 to 66% of the sample and the remaining 34 to 36% is composed of amorphous material. The sharp and narrow peaks show the crystalline structure of clay, while a broad peaks are the sign of an amorphous structure.

Table 3. Mean d spacing of clay

2θ (degree)	d-space (A^o)
12.38	7.14
20.99	4.23
24.98	3.56
26.79	3.32

Table 4. Mean d spacing in clay and composites with RI values

Clay or CUF Composites	2θ (^{o})	d-space (A^o)	RI(%)
Clay	12.38	7.14	-
CUF 5 B	12.25	7.22	1.12
CUF 10 B	12.23	7.29	2.10
CUF 15 B	12.01	7.36	3.08
CUF 20 B	11.44	7.73	8.26
CUF 25 B	11.64	7.60	6.44
CUF 30 B	11.85	7.46	4.4

The peaks as observed in the diffraction pattern of ball clay and corresponding d-space (the interlayer spacing of neat ball clay) are shown in Table 3.

XRD spectrum of CUF composites is shown in Figure 5.

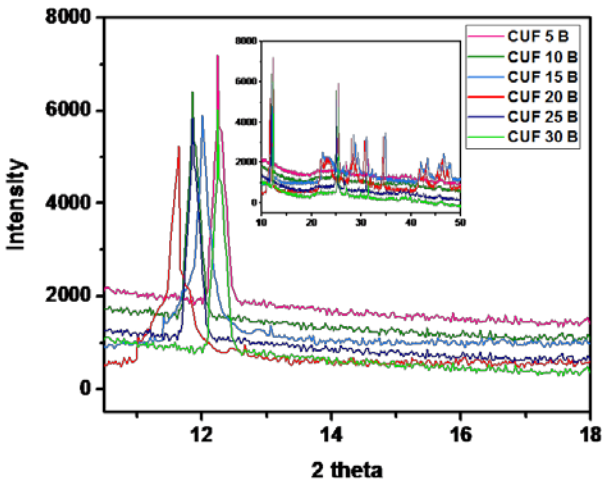

Figure 5. XRD of CUF B composites

The intercalation depth is determined by calculating the inter-gallery spacing, d_{001}, which is present between the polymer and the layered silicates. After mixing this clay with UF resin, the (001) peak is still present, but it shifted to a lower 2θ value corresponds to which d-spacing are given in Table 4. So there was a small but discernible shift downward in diffraction peak angle for all wt% of clay. Therefore clay mixed with UF indicating a small degree of derangement (intercalation) of the crystal structure. This decrease in 2θ value indicates an increase, although relatively small, in the distance between the clay layers.

The calculated d-spacing of clay in the UF resin increased from 7.14A^0 to approximately 7.73A^0. It appears as the intercalation of the UF resin into the clay (meaning a small increase in clay interlayer spacing) to some degree between the clay layers. Incomplete dispersion of clay in UF resin is evidence of some crystalline (partially) clay existing in the resin mix. For UF resin, when mixed with clay, a slightly higher d-spacing in composites could have resulted in monomers of UF resin being smaller and therefore is likely to enter interstitial spaces within the clay particles more easily.

From the data revealed in Table 4, It is evident that intercalation is considerably promoted for different loading levels of clay as positive relative intercalation (RI) values are observed. This is an indication of increment in the clay interlayer space [30]. From the data reported in Table 4, it is concluded that composite CUF 20 B has shown the maximum RI (%) value which means intercalated to a greater extent at 20 wt% loading level of clay.

The crystallinity of clay and CUF composites can be determined by using XRD pattern. To calculate the crystallinity following formula is used.

Crystallinity (%) = Area of crystalline peaks * 100 / Area of all peaks (Crystalline + amorphous)

From XRD patterns, less sharp and less intense crystalline peaks are observed, which approaches the composite towards amorphous nature. Due to this, the crystallinity of the composites decreases compare to clay. Crystallinity in % is given in Table 5. Destruction of the crystallization in the composites is the main reason for the cross linking for building the 3D network structure. In this way, this cross linked network restricts the promotion of crystalline domains, which leads to amorphous structure [31]. The crystallinity and strength of the final product is related. It is stated that the low bonding strength of the three-dimensional network is the result of high crystallinity [32].

Moreover, It is also reported that UF resins' adhesion strength is affected negatively by the formation of crystalline structures within UF resins [33]. The main reason for the poor bonding strength is that the molecules that participated in the crystalline domain's development did not join in cross linked structures and were connected by weak intermolecular bonds [32]. Besides, the lower value of crystallinity could be due to the interaction of particles of clay in UF resins, in which hydrogen-bonded molecules restricted the growth of crystalline domains.

Table 5. Crystallinity of clay and composites

Sample	crystallinity (%)
Clay	70.18
CUF 5 B	65.87
CUF 10 B	61.55
CUF 15 B	57.34
CUF 20 B	51.81
CUF 25 B	62.26
CUF 30 B	63.73

3.3 TGA

Thermo Gravimetric Analysis (TGA) is an analytical technique used to verify a material's thermal stability by observing the mass loss on heating of the sample. This study tries to explain the dispersion of clay in resin. As the temperature increases, corresponding weight loss also occurs due to the release of moisture or gases from the material's decomposition. In the end, only nonvolatile and thermally stable residue remains. The TGA study is done for all CUF composites up to 400°C at a different heating rate (5°C, 10°C, 15°C, 20°C, 25°C). Figure 6 - Figure 12

show the shift in temperature for mass loss values as a function of the heating rate. From the presented TGA curves, it can be seen that the first mass loss step almost occurs between 45°C and 100°C for all samples, which corresponds to a loss of water from the samples. At temperatures, 100°C to 255°C, the broken polymer chains disassembled the network, and cyclic structures in the polymer chain occur. This degradation step results in broad polymer disintegration. The release of formaldehyde from dimethylene ether groups begins with the degradation of cured resins, and the maximum degradation occurred when the stable methylene ether linkages were destroyed [20]. Mass loss occurs from 255°C to 310°C due to dehydration of silane group present in amorphous silica particles. Further above this temperature degradation is due to chemically bound water loss from the SiO_2 particles.

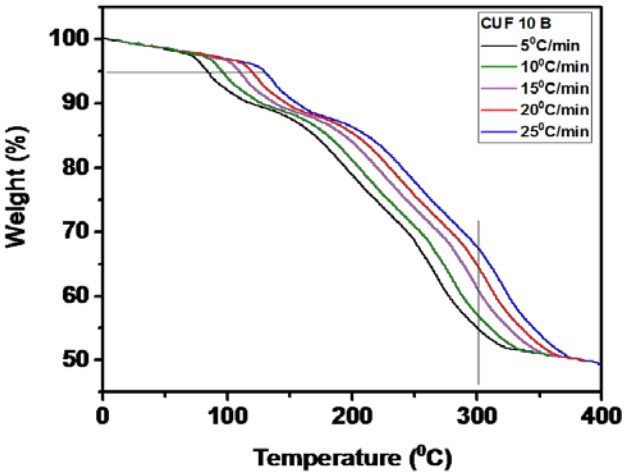

Figure 8. TGA of CUF 10 B composite at different heating rates

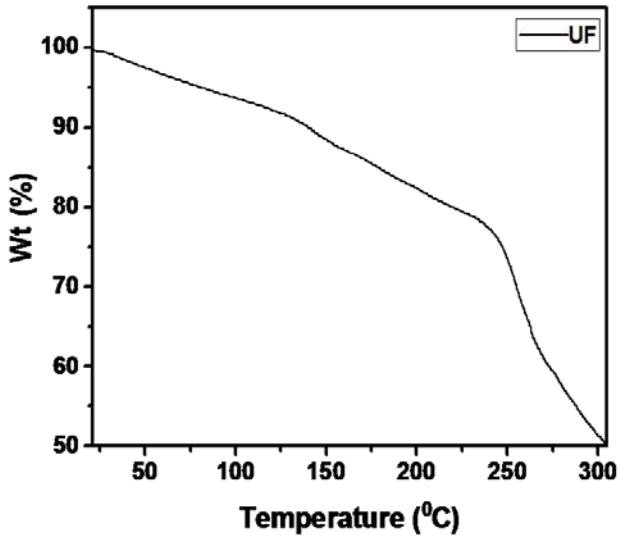

Figure 6. TGA of UF

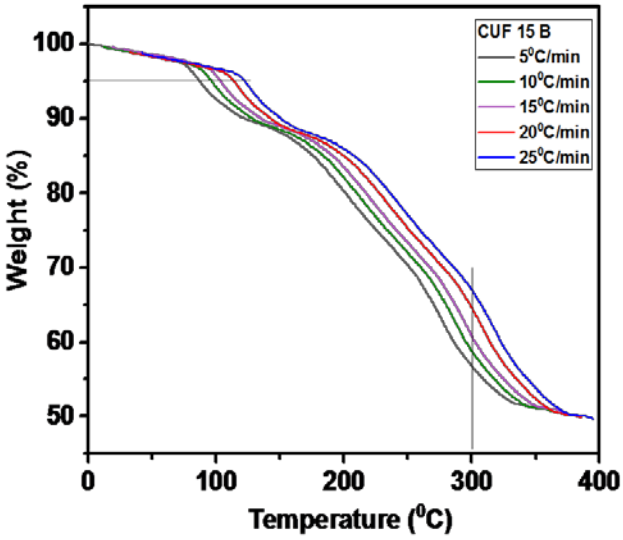

Figure 9. TGA of CUF 15 B composite at different heating rates

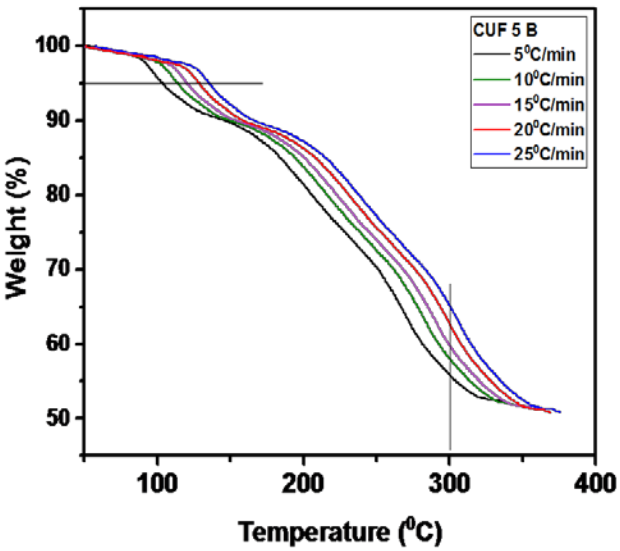

Figure 7. TGA of CUF 5 B composite at different heating rates

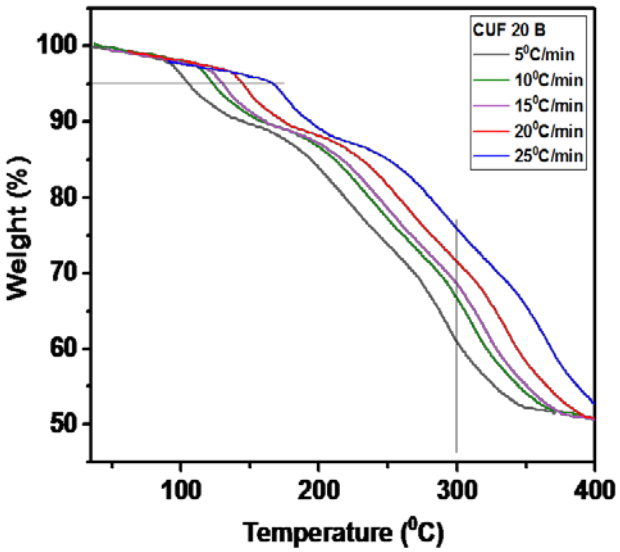

Figure 10. TGA of CUF 20 B composite at different heating rates

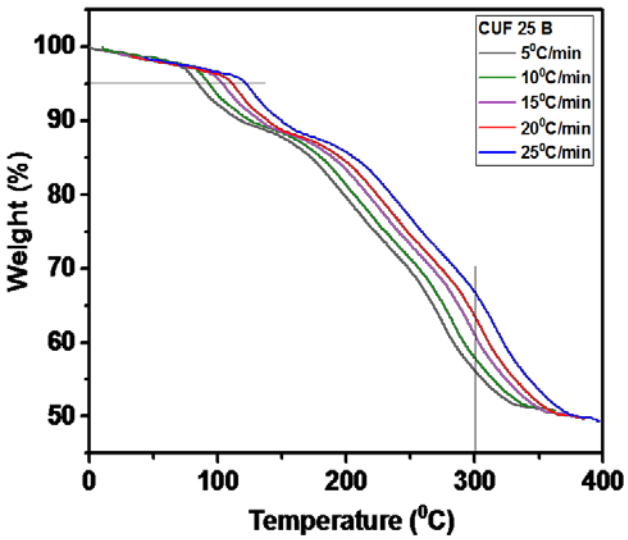

Figure 11. TGA of CUF 25 B composite at different heating rates

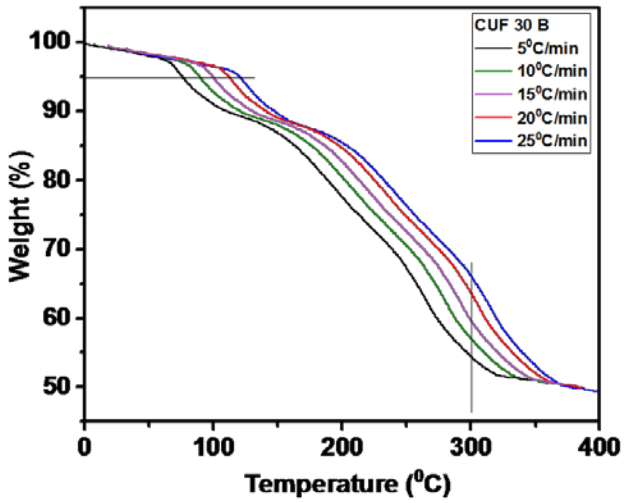

Figure 12. TGA of CUF 30 B composite at different heating rates

As it is said before that TGA gives information about weight loss at a particular temperature. Figure 6 shows the TGA curve for the UF resin and Figures 7-12 show TGA curves for CUF B composites at different heating rates, said above. The temperature for mass loss of 5% for all the composites is shown in Table 6. The observation for thermal stability of the samples can be taken from the TGA curve. Figure 6 shows that for pure UF resin, 5% mass loss occurs at 82°C, while in all composites, it appears at more than 82°C, as shown in Figure 7 – Figure 12. It is concluded here that the thermal stability of composites improved significantly. Similar results are observed at all heating rates. Since the applied heating rate controls the reaction time, which is available at a particular temperature, kinetics degradation directly depends on the heating rate. Generally, it is considered that if the heating rate is lower, the time available for the reaction will be longer. A general trend in the TGA curve is followed that sample degrades at a lower temperature at a lower heating rate, while it decomposes at a higher temperature at a higher heating rate. In this way, thermal stability strongly depends on the heating rate [34]. It is confirmed from Table 6 that as the heating rate increases, the temperature for a particular mass loss (5% mass loss) also increases.

Table 6. Temperature in °C for 5% mass loss at different heating rate

Sample	5°C	10°C	15°C	20°C	25°C
CUF 5 B	103.3	113.12	119.8	127.9	136.18
CUF 10 B	83.1	96.7	109.5	118.9	131.6
CUF 15 B	86.5	96.7	103.6	114.6	121.4
CUF 20 B	105.4	122.5	130.2	145	166.81
CUF 25 B	83.9	92.5	102.7	112	121.8
CUF 30 B	74.6	90	100.2	112.9	120.6

Table 7. Mass residue at 300^{0}C

Sample	5°C	10°C	15°C	20°C	25°C
CUF 5 B	55.84	57.2	59.6	62.5	65
CUF 10 B	54.7	56.6	60.6	64.4	67.4
CUF 15 B	56.7	58.7	60.6	64.8	67.12
CUF 20 B	61.09	66.4	68.7	71.4	76.1
CUF 25 B	56.1	57.75	60.7	63.4	66.9
CUF 30 B	54.42	56.9	59.3	63.3	66.4

At 300°C, From the TG curve, it can be observed that the pure UF produced 51% mass residue, while the composites produced mass residue above 51%, as shown in Table 7. This indicates that the mass residue at a particular temperature is higher for CUF composites. Therefore it is proved that the sample composition CUF B composites are correct as they had been formulated. Among all the composites, CUF 20 B exhibited better thermal stability than pure UF. The better interaction that exists between the components in the composite is the reason behind this stability. Due to the formation of the hydrogen bond, the interaction between clay and UF has been greatly enhanced, and therefore strong adhesion between clay and UF exists.

Further, it is concluded from Table 7 that as the wt% of clay increases up to 20 wt%, the mass residue is higher for all heating rates. The mass residue percentage is high for all CUF composites compared to UF resin, indicating that clay-modified UF composites provide more thermal stability than pure UF resin. This confirms the dispersion between the clay and UF resin.

TGA shows an increase in decomposition temperature in CUF composites which indicates the formation of clay exfoliation or intercalation. This exfoliated or intercalated clay disrupts the polymer decomposition by inhibiting oxygen's movement into the material [35,36]. Hence, it is concluded that any composite's thermal stability is strongly influenced by the morphology and by the loading level of clay particles.

The TGA study indicates that the intercalation or exfoliation of clay in resin shows thermal stability to be better than pure resin. The modified clay has shown better thermal stability, probably due to these reasons.

a. The hydrophilic clay contains SiO_2, which is thermally stable for temperatures up to 500^{o}C, resulting in the enhanced residual weight with 20% of clay. The presence of a higher % of inorganic substance like Sio_2, Fe in clay plays an important role in the thermal stability of CUF composites.

b. When mixed with UF resin, the clay would alleviate UF resin's hydrolysis, which is responsible for this thermal stability.

c. Further, clay has a large surface area; therefore, intercalated or exfoliated clay in composites shows better thermal stability. This is because of the formation of carbonaceous silicate char on the surface during burning. These char layers insulate the underlying material and slow down the escape of volatile products generated during decomposition. So overall, studies show that adding clay will enhance thermal stability.

3.4. DSC

3.4.1. Crystallization Kinetics Phenomenon in DSC Thermal Analysis

The cross linking of polymer molecules in the curing process is exothermic, creating a positive peak in the DSC curve that is usually obtained just after the glass transition. It is known as the crystallization process. The crystallization process occurs above the glass transition temperature. Below the glass transition, molecular mobility is restricted, so there is no crystallization process, and above the glass transition temperature, small crystals are formed at relatively low temperatures. This phenomenon is known as cold crystallization. In the DSC curve, the exothermic peak temperature is considered as crystallization temperature. Usually, activation energy is composed of the activation energy of nucleation E_n and growth energy E_g because nucleation and growth are responsible for the crystallization phenomenon of glasses. Generally, both are combined into activation energy to represent the whole crystallization process. In this study, two theoretical models Ozawa's and Kissinger's equations are used to study crystallization kinetics. Activation energy has been obtained using Kissinger's and Ozawa's model, and their results have been compared in this part.

3.4.2. DSC Thermograms of CUF B Composites

DSC thermograms of CUF B for the above said clay loading level at heating rates 5°, 10°, 15°, 20°, and 25°C/minute has shown in Figure 13-Figure 18.

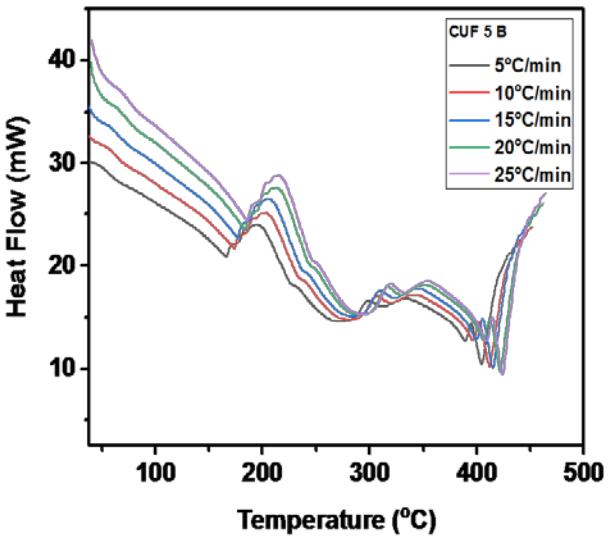

Figure 13. DSC thermograms of CUF 5 B composite

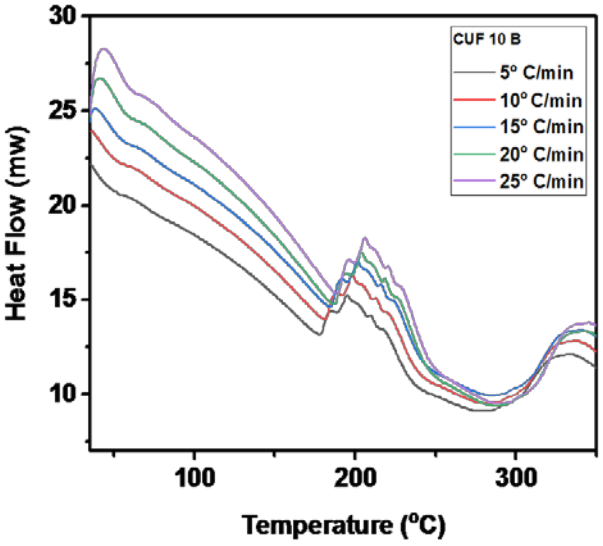

Figure 14. DSC thermograms of CUF 10 B composite

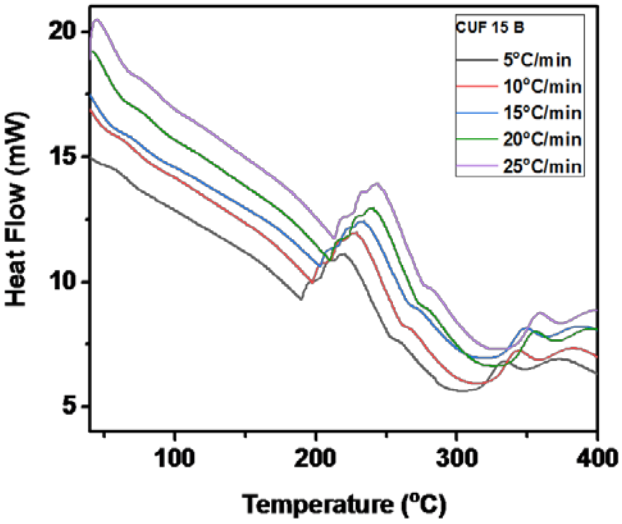

Figure 15. DSC thermograms of CUF 15 B composite

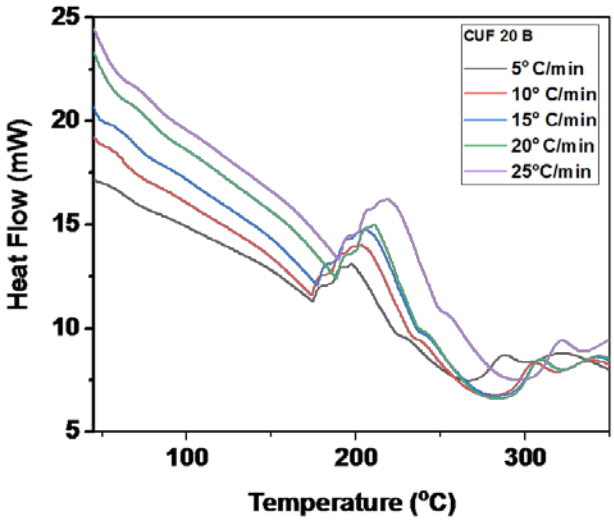

Figure 16. DSC thermograms of CUF 20 B composite

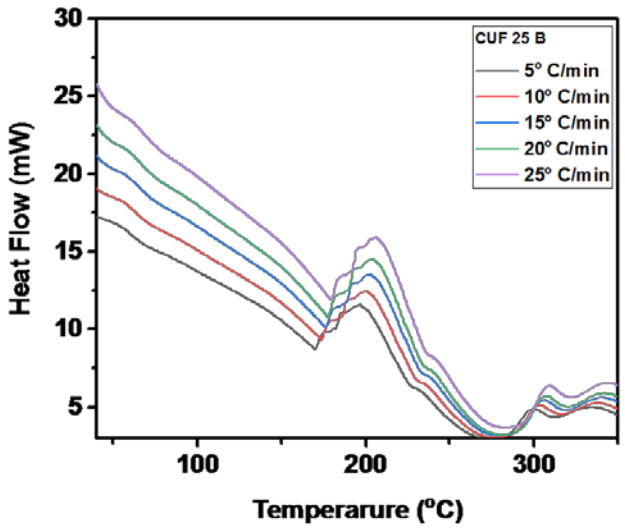

Figure 17. DSC thermograms of CUF 25 B composite

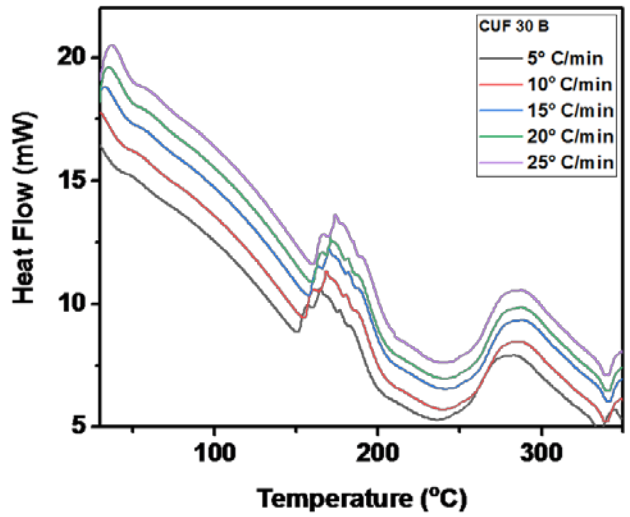

Figure 18. DSC thermograms of CUF 30 B composite

3.4.3. Crystallization Temperature of CUF B Composites

The crystallization phenomenon has been analyzed in terms of crystallization temperature T_c and activation energy E_c. Using DSC thermograms, the value of the composites' crystallization temperature at different heating rates is given in Table 8.

3.4.4. The Crystallization Activation Energy E_c for CUF Composites

On heating again in DSC, crystallization activation energy is the energy absorbed by the atom when it transitions between local potential minima. The energy barriers separate these minima. Among all the local minima, the most stable has the lowest internal energy in the glassy region. Therefore atoms with minimum activation energy have a high probability of making the transition to stable minima and can be stable.

It has been shown [37] that three types of activation energies have to be considered in the crystallization process. These are known as the activation energy of nucleation E_n, the activation energy of growth E_g, the activation energy of whole crystallization process E_c. Again, some studies [38] show that the activation energy for growth may be equal to the activation energy of the whole crystallization if it is evaluated using the sample's thermal analysis. Experimental data are analyzed based on Kissinger's and Ozawa's equation [39] for non isothermal crystallization.

Table 8. Crystallization temperature T_c (°C) for CUF B composites

Heat rate (°C/min)	CUF 5 B	CUF 10 B	CUF 15 B	CUF 20 B	CUF 25 B	CUF 30 B
5	193	197	223	202	192	170
10	199	201	227	205	199	173
15	204	207	232	208	201	178
20	207	211	238	210	203	183
25	212	215	242	217	206	189

3.4.5. The Crystallization Activation Energy for CUF B Composites

Kissinger's model for activation energy

Figure 19 – Figure 24 show the plots of ln (β/T_c^2) as a function of $1000/T_c$ for CUF B composites for different loading levels of clay at the heating rate 5, 10, 15, 20, 25°C/min, respectively. Slope of the straight line gives information about the activation energy in this region for variously said composites and are given in Table 9.

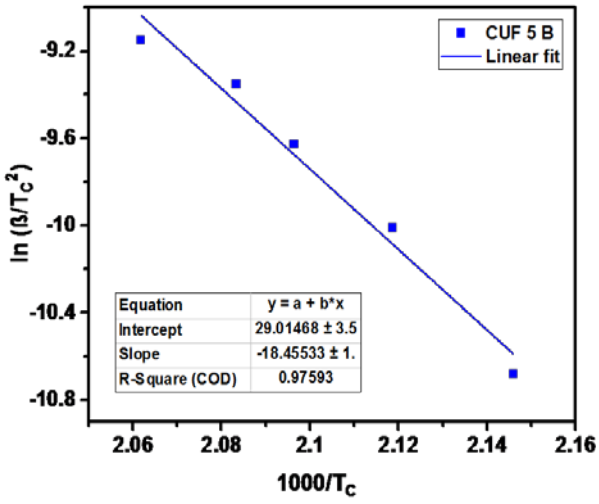

Figure 19. Plot of ln (β/T^2_c) vs $1000/T_C$ for CUF 5 B composite

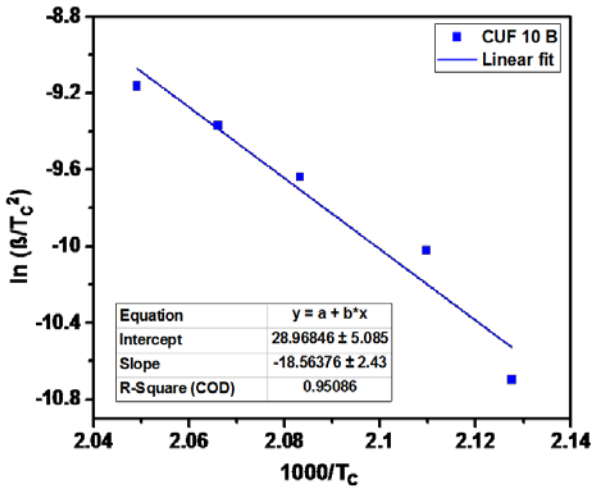

Figure 20. Plot of ln (β/T^2_c) vs $1000/T_C$ for CUF 10 B composite

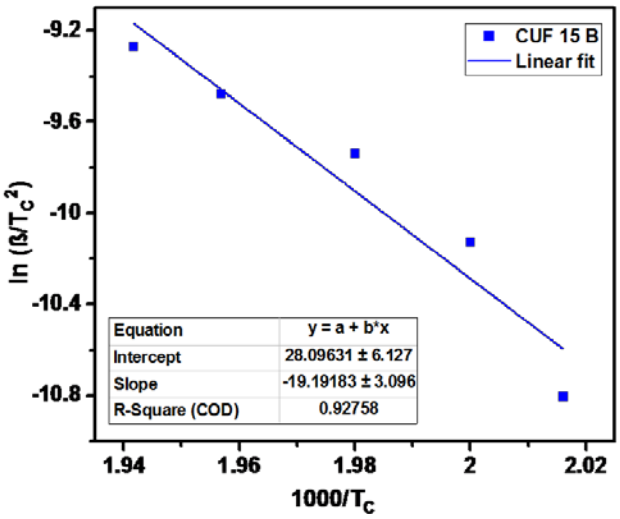

Figure 21. Plot of ln (β/T^2_c) vs 1000/T_C for CUF 15 B composite

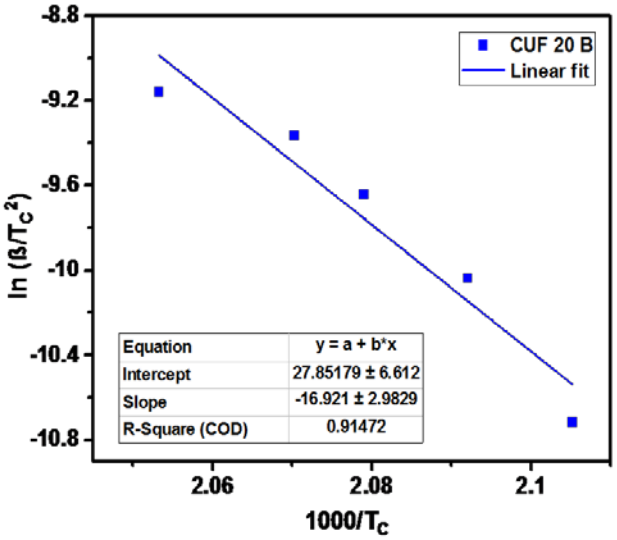

Figure 22. Plot of ln (β/T^2_c) vs 1000/T_C for CUF 20 B composite

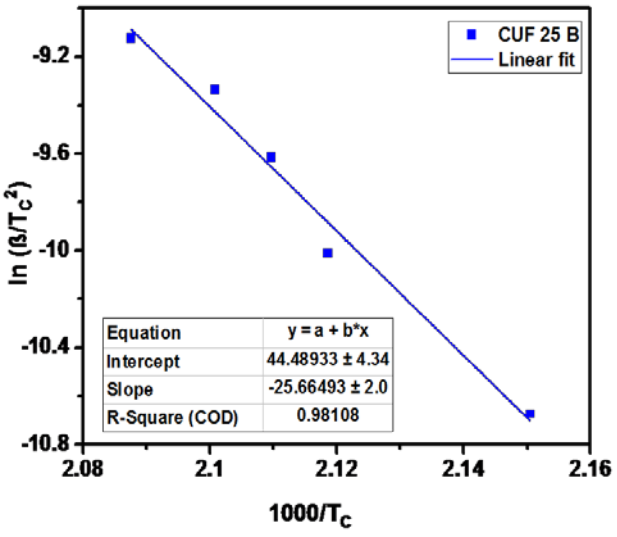

Figure 23. Plot of ln (β/T^2_c) vs 1000/T_C for CUF 25 B composite

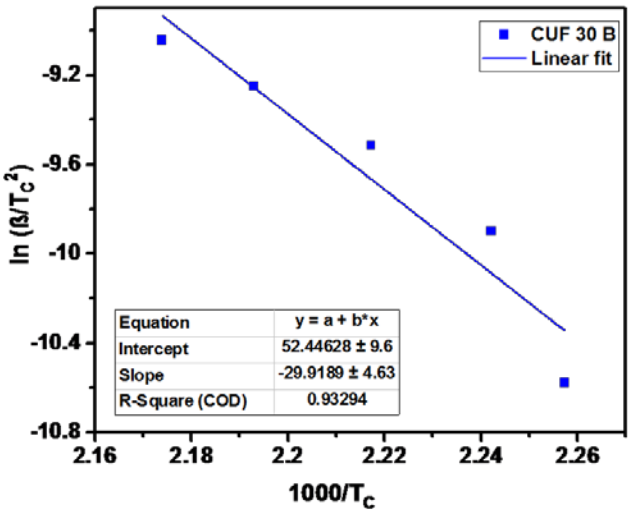

Figure 24. Plot of ln (β/T^2_c) vs 1000/T_C for CUF 30 B composite

Table 9. Crystallization activation energy E_c (KJ/mol)

Sample code	Kissinger's model	Ozawa's model
CUF 5 B	153.36	153.28
CUF 10 B	154.26	154.19
CUF 15 B	159.48	159.57
CUF 20 B	140.61	140.78
CUF 25 B	213.27	210.17
CUF 30 B	248.62	243.92

Ozawa's model for activation energy

Figure 25 - Figure 30 show the plots of ln (β) as a function of 1000/T_c for CUF B composites for different loading levels of clay at the heating rate 5, 10, 15, 20, 25°C/min, respectively. The straight line of obtained curves gives information about the activation energy in this region for variously said composites and is given in Table 9.

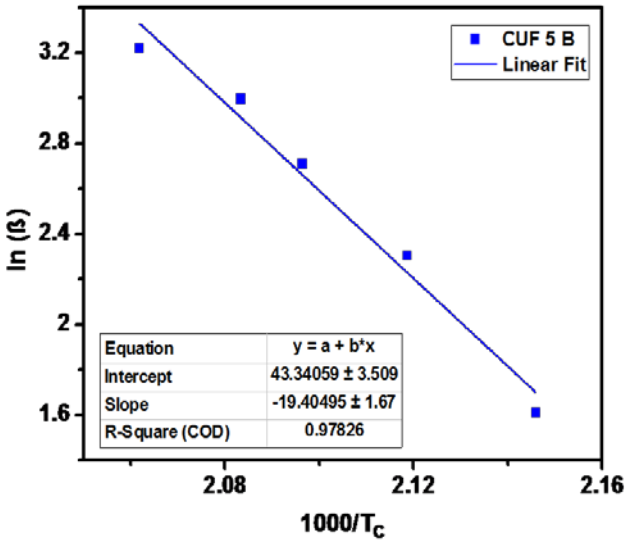

Figure 25. Plot of ln (β) vs 1000/T_c for CUF 5 B composite

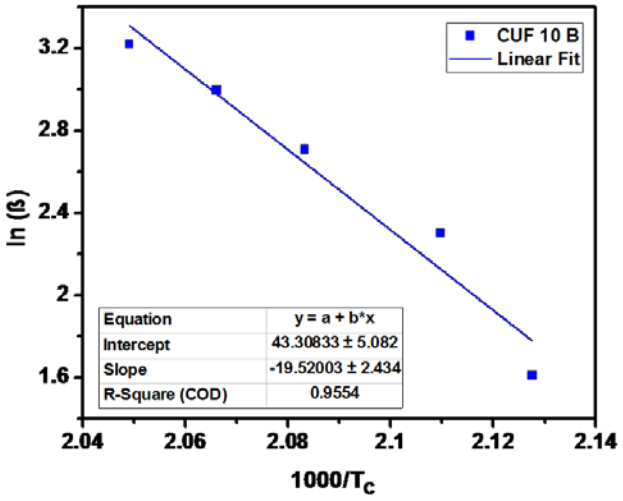

Figure 26. Plot of ln (β) vs 1000/T_c for CUF 10 B composite

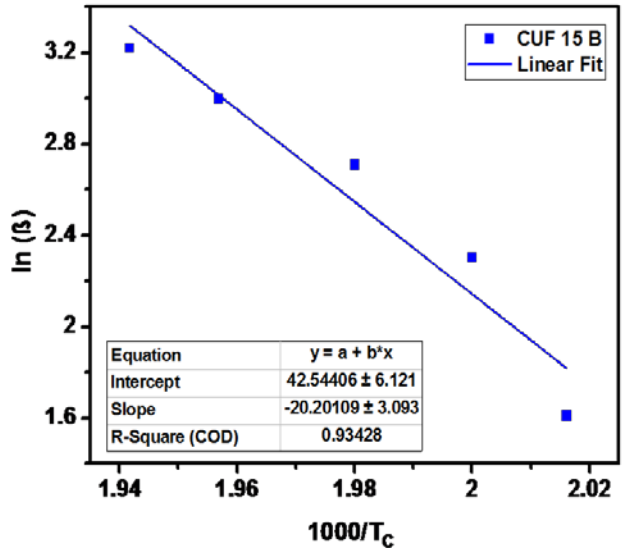

Figure 27. Plot of ln (β) vs 1000/T_c for CUF 15 B composite

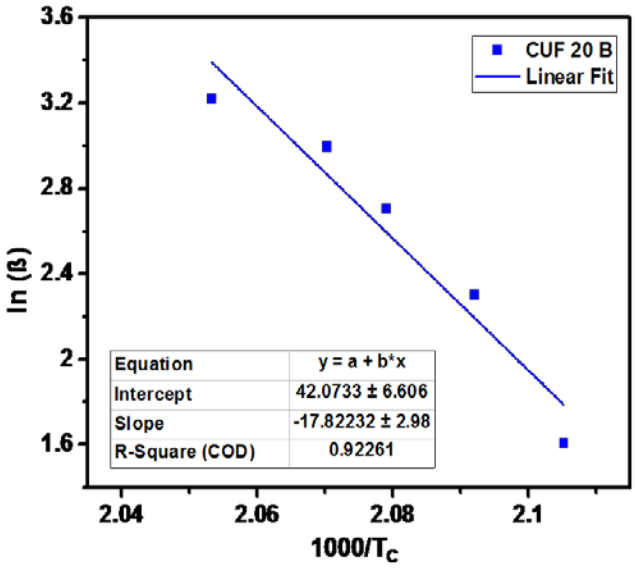

Figure 28. Plot of ln (β) vs 1000/T_c for CUF 20 B composite

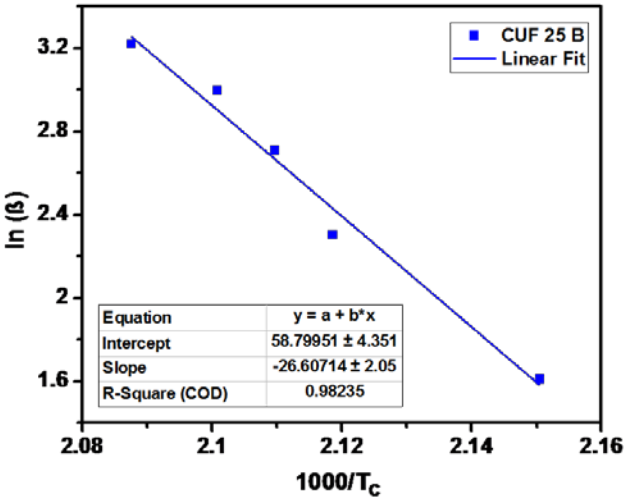

Figure 29. Plot of ln (β) vs 1000/T_c for CUF 25 B composite

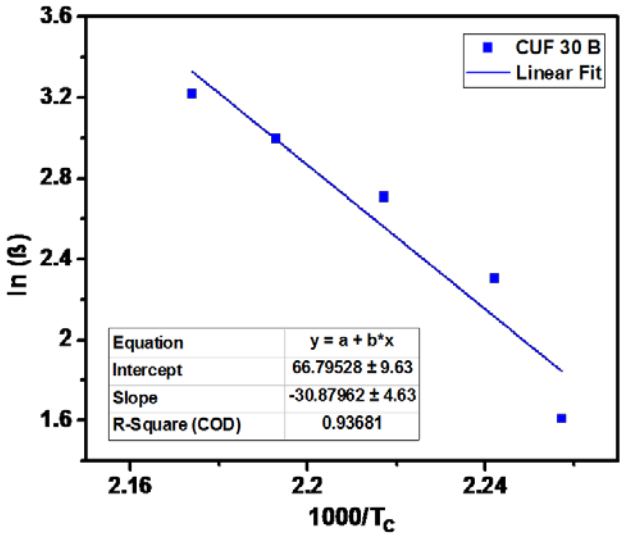

Figure 30. Plot of ln (β) vs 1000/T_c for CUF 30 B composite

It can be seen that for the kinetic analysis of composites, the calculation of the activation energies from Kissinger's and Ozawa's equation are in good agreement, as shown in Table 9. The little difference in the values of activation energies is due to approximations taken to derive these equations. The activation energy is due to the hydrogen bonds forming between the SiO_2 particles of clay and polymer chains of UF resin. The hydrogen bond altered inter phase around particles or aggregate. Hence mobility of the polymer chain, which is needed to cure the UF resin, is less in composites samples with higher activation energy. Therefore they need more energy for the cross linking process.

Further, it is also reported that clay particles create an obstacle that disrupts the matrix's continuity. Therefore, a problem is created for the reactive group of urea and formaldehyde to come close and interact. Thus in this way, the higher activation energy of the curing is an indication of the existence of UF resin/clay particle interactions. Similar results were obtained by other researchers in composites' research work [20,40]. It is clear from Table 9

that composite sample CUF 20 B has the minimum activation energy, which shows that it needs less energy to cure UF resin [41]. XRD results also support this result as the above said composite shows less crystallinity among all the composites shown in Table 5. The reason behind the less crystallinity is the earlier curing of UF resin by the interaction of clay with urea-formaldehyde (UF) resin. Hence, composite does not get enough time to make crystals.

4. Conclusion

1. Clay/urea formaldehyde composites were prepared by varying the clay loading level.
2. FTIR study confirmed the formation of CUF composites.
3. XRD results confirmed the increase in d-spacing of silicate layers, and positive RI values were observed indicating the intercalation of UF resin into clay layers. Composite CUF 20 B showed the maximum d-spacing. Poor crystallinity of CUF 20 B composite also favors a better cross linking network between clay and UF resin, in which hydrogen-bonded molecules restricted the growth of crystalline domains.
4. TGA study revealed that the mass residue percentage is high for all CUF composites compared to UF resin, indicating that clay clay-modified UF composites provide more thermal stability than pure UF resin. It is also found that thermal stability strongly depends on the heating rate and clay loading level.
5. The curing reaction's activation energy has been calculated from DSC thermograms, and it was reported that clay loading level affects the activation energy. Higher activation energy is an indication of the existence of clay/UF composites. Earlier curing and less crystallinity of CUF 20 B composite are observed as it showed minimum activation energy.

References

[1] S Pavlidou and CD Papaspyrides. “A review on polymer–layered silicate nanocomposites”. In: *Progress in polymer science* 33.12 (2008), pp. 1119-1198.

[2] Lei Wang et al. “Preparation, morphology and thermal/mechanical properties of epoxy/nanoclay composite”. In: *Composites Part A: applied science and manufacturing* 37.11 (2006), pp. 1890-1896.

[3] Amit Das et al. “Rubber–clay nanocomposites: some recent results”. In: *Advanced rubber composites*. Springer, 2010, pp. 85-166.

[4] Natacha Bitinis et al. “Recent advances in clay/polymer nanocomposites”. In: *Advanced Materials* 23.44 (2011), pp. 5229-5236.

[5] S Saengsuwan and S Saikrasun. “Thermal stability of styrene–(ethylene butylene)–styrene- based elastomer composites modified by liquid crystalline polymer, clay, and carbon nanotube”. In: *Journal of thermal analysis and calorimetry* 110.3 (2012), pp. 1395-1406.

[6] Zuzana Dujkova, Dagmar Merinska, and Miroslav Slouf. “Fire retardation of polystyrene/clay nanocomposites: Initial study on synergy effect”. In: *Journal of Thermoplastic Composite Materials* 26.9 (2013), pp. 1278-1286.

[7] Hasmukh A Patel et al. “Nanoclays for polymer nanocomposites, paints, inks, greases and cosmetics formulations, drug delivery vehicle and waste water treatment”. In: *Bulletin of Materials Science* 29.2 (2006), pp. 133-145.

[8] David Chu, Quang Nguyen, and Donald G Baird. “Effect of matrix molecular weight on the dispersion of nanoclay in unmodified high density polyethylene”. In: *Polymer composites* 28.4 (2007), pp. 499-511.

[9] Quang T Nguyen and Donald G Baird. “An improved technique for exfoliating and dispersing nanoclay particles into polymer matrices using supercritical carbon dioxide”. In: *Polymer* 48.23 (2007), pp. 6923-6933.

[10] Suprakas Sinha Ray and Masami Okamoto. “Polymer/layered silicate nanocomposites: a review from preparation to processing”. In: *Progress in polymer science* 28.11 (2003), pp. 1539-1641.

[11] Baljinder K Kandola et al. “Effect of different compatibilisers on nanoclay dispersion, thermal stability, and burning behavior of polypropylene–nanoclay blends”. In: *Journal of applied polymer science* 108.2 (2008), pp. 816-824.

[12] Alfred Tcherbi-Narteh et al. “Thermal stability and degradation of di glycidyl ether of bisphenol A epoxy modified with different nanoclays exposed to UV radiation”. In: *Polymer degradation and stability* 98.3 (2013), pp. 759-770.

[13] K Natarajan and KS Anu. “Nanoclay Reinforced polyurethane-epoxy blend: a review”. In: *Int. J. Res. Eng. Adv. Technol* 3.1 (2015), pp. 78-90.

[14] S Martínez Stagnaro, Cristina Volzone, and L Huck. “Nanoclay as adsorbent: evaluation for removing dyes used in the textile industry”. In: *Procedia Materials Science* 8 (2015), pp. 586-591.

[15] Ashraf EM Khater et al. “Natural radionuclides in clay deposits: concentration and dose assessment”. In: *Radiation protection dosimetry* 156.3 (2013), pp. 321-330.

[16] MF Mota et al. “Organophilic clay for oil/water separation process by finite bath tests”. In: *Brazilian journal of petroleum and gas* 5.2 (2011).

[17] R Suresh et al. “Nanoclay drug delivery system”. In: *International Journal of Pharmaceutical Sciences and Nanotechnology* 3.2 (2010), pp. 901-905.

[18] Arimitsu Usuki et al. “Swelling behavior of montmorillonite cation exchanged for ω-amino acids by *Journal of Materials Research* 8.5 (1993), pp.1174-1178.

[19] Dimitris Bikiaris, Vassilis Karavelidis, and George Karayannidis. “A new approach to pre- pare poly (ethylene terephthalate)/silica nanocomposites with increased molecular weight and fully adjustable branching or crosslinking by SSP”. In: *Macromolecular Rapid Communications* 27.15 (2006), pp. 1199-1205.

[20] E Roumeli et al. “Synthesis, characterization and thermal analysis of urea–formaldehyde/nanoSiO2 resins”. In: *Thermochimica Acta* 527 (2012), pp. 33-39.

[21] Sivananda S Jada. “The structure of urea—formaldehyde resins”. In: *Journal of applied polymer science* 35.6 (1988), pp. 1573-1592.

[22] Suzana Samaržija-Jovanović et al. “Thermal behavior of modified urea–formaldehyde resins”. In: *Journal of thermal analysis and calorimetry* 104.3 (2011), pp.1159-1166.

[23] Nilgün Kızılcan and Mehmet Mermutlu. “In situ preparation of cyclohexanone formaldehyde resin/layered silicate nanocomposites”. In: *Journal of Applied Polymer Science* 131.6(2014).

[24] Esin Ateş, Nurseli Uyanık, and Nilgün Kızılcan. “Preparation of urea formaldehyde resin/layered silicate nanocomposites”. In: *Pigment & Resin Technology* (2013).

[25] Ming Liu et al. “Characterization of the crystalline regions of cured urea formaldehyde resin”. In: *RSC advances* 7.78 (2017), pp. 49536-49541.

[26] Brian C Smith. Infrared spectral interpretation: a systematic approach. CRC press, 1998.

[27] BS Mamatha. “Studies on nanoclay based multi particle layered biocomposite”.

[28] Qiaojia Lin et al. “Property of nano-SiO 2/urea formaldehyde resin”. In: *Frontiers ofForestry in China* 1.2 (2006), p. 230.

[29] Ahmet Gürses et al. “Investigation of Thermal Properties of PUF/colored Organoclay Nanocomposites”. In: *Acta Physica Polonica A* 4.127 (2015), pp. 979-983.

[30] Rhutesh K Shah and Donald R Paul. “Organoclay degradation in melt processed polyethylene nanocomposites”. In: *Polymer* 47.11 (2006), pp. 4075-4084.

[31] Emiko Otsuka et al. “Effects of microcrystallites on swelling behavior in chemically crosslinked poly (vinyl alcohol) gels”. In:

Journal of Polymer Science Part B: Polymer Physics 49.2 (2011), pp. 96-102.

[32] EE Ferg, A Pizzi, and DC Levendis. “13C NMR analysis method for urea–formaldehyde resin strength and formaldehyde emission”. In: *Journal of Applied Polymer Science* 50.5 (1993), pp. 907-915.

[33] A Despres and A Pizzi. “Colloidal aggregation of aminoplastic polycondensation resins: Urea– formaldehyde versus melamine-formaldehyde and melamine–urea–formaldehyde resins”. In: *Journal of applied polymer science* 100.2 (2006), pp. 1406-1412.

[34] Henry Kuo Feng Cheng et al. “Thermal kinetics of montmorillonite nanoclay/maleic anhydride- modified polypropylene nanocomposites”. In: *Journal of thermal analysis and calorimetry* 109.1 (2012), pp. 17-25.

[35] John Cuppoletti. Nanocomposites and polymers with analytical methods. BoD–Books on Demand, 2011.

[36] Fouad Laoutid et al. “New prospects in flame retardant polymer materials: from fundamentals to nanocomposites”. In: *Materials Science and Engineering: R: Reports* 63.3 (2009), pp. 100-125.

[37] Kazumasa Matusita, Takayuki Komatsu, and Ryosuke Yokota. “Kinetics of non-isothermal crystallization process and activation energy for crystal growth in amorphous materials”. In: *Journal of Materials Science* 19.1 (1984), pp. 291-296.

[38] Roger L Blaine and Homer E Kissinger. “Homer Kissinger and the Kissinger equation”. In: *Thermochimica acta* 540 (2012), pp. 1-6.

[39] K Ozawa. “Estimating isothermal life from thermogravimetric data”. In: *Bull Chem Soc Jpn* 38 (1966), pp. 1881-4.

[40] A Manzur and F Hernández-Sánchez. “Activation energy for the glass transition of a confined elastomer in HDPE/PP blends”. In: *Journal of Macromolecular Science, Part B: Physics* 45.1 (2006), pp. 139-152.

[41] Junling Yuan, Xiaowen Zhao, and Lin Ye. “Structure and properties of urea-formaldehyde resin/polyurethane blend prepared via in-situ polymerization”. In: *RSC Adv*.